

Landau Theory of Free Standing and Epitaxial Ferroelectric Film

by

Ahmad M. A. Musleh

Thesis submitted in fulfillment of the
requirements for the degree of
Doctor of Philosophy

May 2009

ACKNOWLEDGEMENTS

I gratefully acknowledge my supervisors Dr Ong Lye Hock and Prof. Junaidah Osman for their insight, encouragement and guidance throughout this research project. They have given me the continuous motivation, assistance and concerns in supervising my work. I would like to express my sincere gratitude to Prof. David Reginald Tilley for his many valuable suggestions; and I am also grateful to Prof. Yoshihiro Ishibashi for his valuable suggestions. To all members of theoretical group, I would also like to acknowledge them especially Mr. Tan Ten Yong and Mr. Wong Ten It. I would like to thank the Academy of Sciences Malaysia for the SAGA grant (Grant No: 304/PFIZIK/653018/A118) to finance the project and the Post Graduate Student Centre, USM for granting me a fellowship. Of course I cannot forget my parents for their prayers during my study. To my wife and children who stay with me in Malaysia during my studies, I am thankful for their patience and supports they have given to me that encourage me to go on. I would like to present this thesis to my original home village, Yallo in Palestine and also to my home country, Jordan.

TABLES OF CONTENTS

Acknowledgment	ii
Table of Contents	iii
List of Tables	viii
List of Figures	ix
Abstrak	xix
Abstract	xxii
CHAPTER 1 AN OVERVIEW	
1.1 Introduction	1
1.2 Thesis Overview	4
CHAPTER 2 GENERAL PHYSICS OF FERROELECTRIC	
2.1 Definition of Ferroelectricity	6
2.2 Brief History of Ferroelectricity	7
2.3 Ferroelectric Domains.....	9
2.4 Switching Phenomenon.....	14
2.5 Classification of Ferroelectric Materials.....	17
2.5.1 Displacive Ferroelectrics.....	18
2.5.2 Order-Disorder Ferroelectrics.....	21
2.5.2.(a) Potassium Dihydrogen Phosphate KH_2PO_4	21
2.5.2.(b) Triglycine Sulfate $(\text{CH}_2\text{NH}_2\text{COOH})_3 \cdot \text{H}_2\text{SO}_4$	23
2.6 Theories of Ferroelectric Phase Transition.....	23
2.6.1 Lattice Dynamic Theory of Ferroelectrics	23

2.6.2	Landau Theory	26
2.6.2.(a)	Second-Order Phase Transition	27
2.6.2.(b)	First-Order Phase Transition	31
2.7	Application of Ferroelectrics	34
2.7.1	Dielectric Application	34
2.7.2	Applications of Polarization Reversal	35
2.7.3	Electro Optic Application.....	38
2.7.3.(a)	Application of Ferroelectric Thin Film As Waveguides.....	38
2.7.3.(b)	Ferroelectric Thin Film As Optical Memories.... and Optical Displays	39

CHAPTER 3 REVIEW OF SWITCHING PHENOMENA AND EPITAXIAL FILM OF FERROELECTRIC

3.1	Introduction	40
3.2	Review on Experimental Studies of Polarization reversal.....	40
3.3	Theoretical studies of polarization reversal	46
3.3.1	Statistical Treatment of Polarization Reversal	47
3.3.2	Polarization reversal based on Landau-type free energy	52
3.3.3	Landauer Model	55
3.4	Review of Epitaxial Film Properties	57
3.4.1	Experimental studies of Epitaxial Film	57
3.4.2.	Theoretical studies of Epitaxial Film	61

CHAPTER 4 POLARIZATION REVERSAL IN FERROELECTRIC THIN FILM ACCORDING TO THE TILLEY- ZEKs-MODEL

4.1	Introduction	65
4.2	Theory and Modeling	66
4.3	Numerical Method	69
4.4	Polarization Profile	74
4.5	Switching Properties of Second-Order Ferroelectrics Film	74
4.5.1	Polarization Reversal under Step Electric Field	74
4.5.1.(a)	Surface Effect on Polarization Reversal	76
4.5.1.(b)	The Effect of Temperature on Polarization Reversal ..	81
4.5.1.(c)	The Effect of Electric Field on Polarization Reversal..	83
4.5.1.(d)	Ferroelectric Coercive Field	87
4.5.1.(e)	The Effect of Film Thickness on Polarization Reversal	93
4.5.1.(f)	Evolution of Polarization Profile during Switching ...	98
4.5.2	Switching under Bipolar Pulse Electric Field	104
4.5.3	Polarization Reversal under Sinusoidal Electric Field	105
.....		
CHAPTER 5 SWITCHING REVERSAL OF FERRELECTRIC SYSTEMS OF FINITE SIZE		
5.1	Introduction	113
5.2	The Model and Boundary Condition	114
5.3	Numerical Analysis.....	118
5.4	Results and Discussion	118
CHAPTER 6 SWITCHING BEHAVIOUR OF FERROELECTRIC SYSTEMS WITH A ZERO-SURFACE POLARIZATION		
6.1	Introduction	125
6.2	Theory and Modeling	125

6.3 Numerical Methods.....	126
6.4 Polarization Reversal under Step Electric Field	127
6.5 Switching Under Triangular applied field	138
 CHAPTER 7 EFFECT OF COMPRESSIVE STRESS ON BARIUM TITANATE BaTiO₃ FERROELECTRIC EPTAXIAL FILM	
7.1 Introduction	142
7.2 Free Energy of Strained BaTiO ₃ Thick Film	144
7.3 Physical Conditions and Free Energy of Epitaxial BaTiO ₃ Thin Film...	148
7.4 Numerical Technique	152
7.5 Results and Analysis	153
7.5.1 Compressive Stress Effect on Average Polarization of BaTiO ₃ Film	153
7.5.2 Effect of Compressive Stress on Transition Temperature of BaTiO ₃ Film.....	159
7.5.3 Polarization Profile and Entropy of Strained BaTiO ₃ Film	161
 CHAPTER 8 SUMMARY AND POSSIBLE EXTENTIONS	
8.1 Summary	165
8.2 Possible Extension	168
REFERENCES	173
 APPENDIX A	
Terminology of Stress	188
Terminology of Strain.....	189
 APPENDIX B The flow-Chart on Simulation of the Initial Polarisation Profile in Chapter 4, 5, and 7.....	
	191

APPENDIX C	The Flow-Chart on Simulation of the Polarisation	
	Profile during Switching for Chapter 4 and 5.....	192
APPENDIX D	The Flow-Chart on Simulation of Initial Polarisation	
	Profile and Polarisation during Switching for Chapter 6.....	193
LIST OF PUBLICATION	194

LIST OF TABLES

	Page
Table 2.1 Domain wall configurations: a comparison between ferromagnetic and ferroelectric domain	12
Table 4.1 Regression analysis of the numerical data in Fig. 4.16	91
Table 4.2 Regression analysis of the numerical data in Fig. 4.18	93

LIST OF FIGURES

		Page
Figure 2.1	Schematic diagram of domain arrangements in (001) plate of tetragonal BaTiO ₃ . Arrows represent the direction of the polar axis. (a) is for 'a' domain between 'c' domains, (b) is 'a' domains only.	10
Figure 2.2	Schematic diagram of antiparallel domains formed as a result of depolarization field E_d (thick arrows) due to bound charges on surfaces. Thin arrows are for P_S . Surfaces here are the domain boundary of ferroelectric without external electrodes.	11
Figure 2.3	Schematic diagram showing the difference between ferromagnetic and ferroelectric 180° domains. (a) for ferromagnetic, (b) for ferroelectric. The layer between the dotted lines is the thickness of the domain wall (Jona and Shirane, 1962).	12
Figure 2.4	Schematic diagram of domain walls for tetragonal BaTiO ₃ . (a-a') is 180° wall, (b-b') are 90° wall (Jona and Shirane, 1962).	13
Figure 2.5	One dimensional fictitious crystal (Jona and Shirane, 1962)	14
Figure 2.6	Schematic diagram of double potential wells	14
Figure 2.7	Schematic representation of P - E hysteresis loop of a second order ferroelectric material. The double potential wells represents the polarization state during switching.	15
Figure 2.8	Cubic perovskites-type structure.	19
Figure 2.9	Three phase transitions of BaTiO ₃ . (a) change of polarisation direction from non polar (cubic) to [001] (tetragonal) to [011] (monoclinic) to [111] (rhombohedral) directions, while (b) the temperature dependence of spontaneous polarisation for the three transitions. The source of (b) from (Strukov and Levanyuk, 1998).	20
Figure 2.10	Structure of KH ₂ PO ₄ (KDP) in paraelectric phase.	22
Figure 2.11	PO ₄ tetrahedron of KDP structure with hydrogen bonds to the nearest neighbours.	22

Figure 2.12	Temperature dependence of spontaneous polarisation in second-order phase transition.	30
Figure 2.13	Free-energy versus the polarization at different temperature for second-order transition.	31
Figure 2.14	Spontaneous polarisation versus the temperature for first-order phase transition. The three transition temperatures: T_0 (T_{SC}), T_C , T_{SH} are shown. The values of the transition temperatures and P_S are in reduced form based on a scale of Tan <i>et al.</i> (2001a).	33
Figure 2.15	Free energy as a function of polarization for different temperature for first-order transition.	34
Figure 4.1	Polarization $p(\zeta)$ versus ζ for positive extrapolation length $\delta_r = 0.1$ (solid curve), 3.0 (dashed curve) and 100.0 (dotted curve). $l = 5.0$, $t = 0.0$, $e = 0.0$.	73
Figure 4.2	Polarization $p(\zeta)$ versus ζ for negative extrapolation length $\delta_r = -1.4$ (solid curve), -3.0 (dashed curve) and -100.0 (dotted curve). $l = 5.0$, $t = 0.0$, $e = 0.0$.	74
Figure 4.3	Time dependence of average polarization \bar{p} for positive extrapolation length $\delta_r = 0.1$ (solid curve); 3.0 (dashed curve) and 100 (dotted curve). $l = 5.0$, $t = 0.0$, $e = 10.0$. The inset shows the corresponding switching current.	76
Figure 4.4	Time dependence of average polarization \bar{p} for positive extrapolation length $\delta_r = 0.1$ (solid curve); 3.0 (dashed curve) and 100 (dotted curve). $l = 5.0$, $t = 0.0$, $e = 1.1$. The inset shows the corresponding switching current.	77
Figure 4.5	Time dependence of average polarization \bar{p} for negative extrapolation length $\delta_r = -1.4$ (solid curve), -3.0 (dashed curve) and -100 (dotted curve). $l = 0.72$, $t = 0.0$, $e = 10.0$. The inset shows the corresponding switching current.	77
Figure 4.6	Positive extrapolation length dependence of switching time for thicknesses $l = 0.72$ (circle) and 5.0 (triangle). $t = 0.0$, $e = 10.0$.	78
Figure 4.7	Negative extrapolation length dependence of switching time for	79

- thicknesses $l = 0.72$ (circle) and 5.0 (triangle). $t = 0.0$, $e = 10.0$. The inset shows the zoom in view for a range of $|\delta| \leq 40$.
- Figure 4.8 Coercive field versus positive extrapolation length for film thicknesses $l = 0.72$ (circle) and 5.0 (triangle). $t = 0.0$. **79**
- Figure 4.9 Coercive field versus negative extrapolation length for film thicknesses $l = 0.72$ (circle) and 5.0 (triangle). $t = 0.0$. The inset shows the zoom in view for a range of $|\delta| \leq 40$. **80**
- Figure 4.10 Average polarization versus time for temperatures $t = 0.0, 0.2$ and 0.4 . $l = 1.8$, $\delta_r = +3.0$, $e = 1.0$. The inset shows the corresponding switching current. **82**
- Figure 4.11 Average polarization versus time for temperature $t = 0.0, 0.5$, and 1.2 . $l = 2.7$, $\delta_r = -3$, $e = 2.0$. The inset shows the corresponding switching current. **83**
- Figure 4.12 Average polarization versus time for electric fields $e = 0.5, 0.8, 1.01$ and 1.2 . $l = 1.8$, $\delta_r = +3.0$, $t = 0.0$. The inset shows the switching time versus applied field e . The arrow inside the inset indicates the film coercive field e_{cf} . **84**
- Figure 4.13 Switching current versus time for $e = 0.5, 0.8, 1.01$ and 1.2 . $l = 1.8$, $\delta_r = +3.0$, $t = 0.0$. This figure corresponds to the Fig. 4.12. **85**
- Figure 4.14 Average polarizations versus time for different values of e as noted in the figure. $l = 0.72$, $\delta_r = -2.0$, $t = 0.5$. The inset shows the switching time versus applied field e . The arrow indicates the film coercive field e_{cf} . **86**
- Figure 4.15 4.15 Switching current versus time for $e = 10.0, 9.0, 8.5, 8.3$ and 7.8 of e_{cb} . $l = 0.72$, $\delta_r = -2.0$, $t = 0.5$. This figure corresponds to the Fig. 4.14. **86**
- Figure 4.16 Electric field dependence of switching time for film thickness $l = 2.0$, $\delta_r = +3.0$, $t = 0.0$. Numerical data (Triangle). The three formulation used to fit the numerical data are $\tau_s = k/(e - \alpha)$ (solid curve), $\tau_s = \tau_0 \exp[a/(e - b)]$ (dotted curve) and $\tau_s = \tau_0 \exp(\beta/e)$ (dashed curve). The inset shows the zoom in view for a range of $e_{cf} \leq e \leq 0.8$. **90**
- Figure 4.17 Natural logarithm of switching time $\ln \tau_s$ versus reciprocal **91**

electric field $1/e$ for formulation $\tau_s = k/(e - \alpha)$ (solid curve), $\tau_s = \tau_0 \exp[a/(e - b)]$ (dotted curve), $\tau_s = \tau_0 \exp(\beta/e)$ (dashed curve) and the numerical simulation data of Fig. 4.16 (dashed-double dot curve). The inset (a) shows the reciprocal switching time versus e .

- Figure 4.18 Switching time τ_s versus applied electric field e for dimensionless thickness $l = 2.0$, extrapolation length $\delta_r = -3$, and $t = 0.0$. The triangle in (a), (b), and (c) is used to represent the numerical data points. The data are fitted by $\tau_s = \tau_0 \exp[a/(e - b)]$ (a), $\tau_s = k/(e - \alpha)$ (b) and $\tau_s = \tau_0 \exp(\beta/e)$ (c). **92**
- Figure 4.19 Switching time τ_s versus applied electric field e for film thicknesses $l = 1.0, 2.0, 4.0$, and 6.75 . $\delta_r = +3.0, t = 0.0$. The arrow shows the direction of increasing film thickness. **93**
- Figure 4.20 Switching time τ_s versus applied electric field e for film thicknesses $l = 1.0, 2.0, 4.0$, and 5.67 . $\delta_r = -3, t = 0.0$. The arrow shows the direction of increasing film thickness. **94**
- Figure 4.21 Coercive field e_{cf} versus film thickness l for positive extrapolation length $\delta_r = 3.0$ (Triangle), 10.0 (circle) and 50.0 (square). $t = 0.0$. The dashed line is the value of bulk coercive field e_{cb} . **95**
- Figure 4.22 Coercive field e_{cf} versus film thickness l for negative extrapolation length $\delta_r = -3.0$ (triangle), -10.0 (circle) and -50.0 (square). $t = 0.0$. The dashed line is bulk coercive field value $e_{cb} = 1.0$. The inset shows the zoom in view for a range of $l \leq 3$. **96**
- Figure 4.23 Switching time τ_s versus film thickness l for positive extrapolation length $\delta_r = 3.0$ (Triangle), 10.0 (circle) and 50 (square). $e = 2.0, t = 0.0$. **97**
- Figure 4.24 Switching time τ_s versus film thickness l for negative extrapolation length $\delta_r = -3.0$ (Triangle), -10.0 (circle) and -50.0 (square). $e = 25.0, t = 0.0$. **98**
- Figure 4.25 Polarization profile $p(\zeta)$ during switching for thick film. $l = 5.0, \delta = +1.3, e = 1.7, t = 0.0$. The number at each curve represents time taken to reach the stage in terms of fraction of **99**

$$\tau_s = 3.77.$$

- Figure 4.26 Polarization profile $p(\zeta)$ during switching for thin film. $l = 1.44$, $\delta_r = +1.3$, $e = 1.7$, $t = 0.0$. The number at each curve represents time taken to reach the stage in terms of fraction of $\tau_s = 2.569$. **100**
- Figure 4.27 Switching current versus time for film center (solid curve) and film surface (dashed curve) of film thickness $l = 5.0$. $\delta_r = +1.3$, $e = 1.7$, $t = 0.0$. The inset shows the corresponding polarization evolution. **100**
- Figure 4.28 Polarization profile $p(\zeta)$ during switching for thick film. $l = 5.0$, $\delta_r = -1.3$, $e = 1.7$, $t = 0.0$. (Film parameters are the same as that of thick film with $+\delta_r$, see Fig. 4.25). Polarization profile stages taken from bottom to top at 0.0, 0.1, 0.2, 0.4, 0.6, 0.8, 0.9, 0.92, 0.94, 0.96, 0.98, 0.99, and 1.0 in terms of fraction of $\tau_s = 14.615$. **101**
- Figure 4.29 Switching current versus time at film surface (S) and at film center (C) for thick film. $l = 5.0$, $\delta_r = -1.3$, $e = 1.7$, $t = 0.0$. The inset shows the corresponding polarization evolution. **102**
- Figure 4.30 Polarization profile $p(\zeta)$ during switching for thin film. $l = 1.44$, $\delta = -1.3$, $e = 3.5$, $t = 0.0$. (Film parameters are the same as that for thin film with $+\delta$, but at higher e (Fig. 4.26)). Polarization profile stages taken from bottom to top at 0.0, 0.1, 0.7, 0.85, 0.9, 0.92, 0.94, 0.96, and 1.0 in terms of fraction of $\tau_s = 12.17$. **103**
- Figure 4.31 Average Polarization (dashed curve) and switching current (solid curve) versus time. Using bipolar pulse field. $l = 1.8$, $\delta_r = +3.0$, $e = 1.0$, $t = 0.0$. τ_s is the switching time, τ_w is the pulse width. **104**
- Figure 4.32 Hysteresis loops for various sinusoidal electric field amplitude e_0 . The insets from *a* to *f* show the separate hysteresis loop of this figure for $e_0 = 0.8450000$ (*a*), $e_0 = 0.8461050$ (*b*), $e_0 = 0.8461100$ (*c*), $e_0 = 0.8500000$ (*d*), $e_0 = 1.0$ (*e*) and $e_0 = 1.5$ (*f*). Inset *g* shows the zoom in view for the unclear right lower portion of hysteresis loops indicated by arrow. $l = 5.0$, $t = 0.0$, $\delta_r = +3.0$, $\omega = 0.01$. $e_0 = 1.5$ (*f*). Inset *g* shows the zoom in view for the unclear right lower portion of hysteresis loops indicated by arrow. $l = 5.0$, $t = 0.0$, $\delta_r = +3.0$, $\omega = 0.01$. **106**

Figure 4.33	Hysteresis loops for sinusoidal electric field amplitude $e_0 = 0.800000, 0.850000, 0.905800, 0.905890, 0.905897, 0.905898, 0.905900, 0.910000, 1.000000, 1.500000$ and 2.000000 from a to k respectively. $l = 5.0, t = 0.0, \delta_r = +3, \omega = 0.08$. The film parameters are the same as that in Fig.4.32 but the field is at higher frequency than that in Fig. 4.32.	107
Figure 4.34	Hysteresis loops for sinusoidal electric field amplitude $e_0 = 0.6, 1.0$ and 2.0 . $l = 1.35, \delta_r = +3, t = 0.0, \omega = 0.09$.	108
Figure 4.35	Hysteresis loops for sinusoidal electric field frequencies $\omega = 0.03, .09, 0.20, 0.30$. Curve a for $\omega = 1.2$. $l = 1.35, t = 0.0, \delta_r = +3.0, e_0 = 2.5$.	109
Figure 4.36	Hysteresis loops for temperatures $t = 0.0, 0.2,$ and 0.6 . $l = 2.0, e_0 = 3.0, \omega = 0.1$. (a) for FE film with $\delta_r = +3.0,$ (b) for FE film with $\delta_r = -3$.	110
Figure 4.37	Hysteresis loops for various extrapolation lengths: (a) for $\delta_r = 3.0, 10.0, 50.0,$ (b) for $\delta_r = -3.0, -10.0,$ and -50.0 . $l = 0.72, t = 0.0, e_0 = 3.0, \omega = 0.1$.	111
Figure 4.38	Hysteresis loops for film thicknesses $l = 0.72, 2.0,$ and 5.0 . $e_0 = 3.0, \delta_r = 10.0, \omega = 0.1, t = 0.0$.	112
Figure 4.39	Hysteresis loops for film thicknesses $l = 0.72, 2.0,$ and 5.0 . $e_0 = 3.0, \delta_r = -10.0, \omega = 0.1, t = 0.0$.	112
Figure 5.1	Schematic diagram of one dimensional ferroelectric system of finite size. L is the size of the finite system	114
Figure 5.2	Average polarization versus time for system of finite size under applied electric field $e = 0.2, 0.4, 0.5$ and 0.6 . $l = 2.7, \delta_r = +4.0, t = 0.3$. The arrow inside the inset indicates e_{cf} of the system of finite-sized	119
Figure 5.3	Switching current versus time for system of finite size with $l = 2.7, \delta_r = +4.0$ and $t = 0.3$ under applied electric field $e = 0.2, 0.4, 0.5$ and 0.6 which corresponds to Fig. 5.2.	120
Figure 5.4	Time dependence of spontaneous polarization for FE system of finite size at the edges (dotted curve) and at the center (dashed curve). Solid curve is the average spontaneous polarization.	120

$l = 1.8, \delta_r = +3.0, t = 0.0$ and $e = 0.8$.

- Figure 5.5 Time dependence of switching current which corresponds to polarisation in Fig. 5.4 for the finite size system with $l = 1.8, \delta_r = +3.0, t = 0.0$ and $e = 0.8$ at the edges (dotted curve) and at the center (dashed curve). Solid curve is the switching current of average polarization. **121**
- Figure 5.6 Polarization profiles during switching at various times in terms of fraction of the switching time τ_s at temperature $t = 0.5$, extrapolation length $\delta_r = 2.0, l = 4.5, e = 0.3$. The number at each curve represents time taken to reach the stage in terms of fraction of τ_s . **122**
- Figure 5.7 Polarization profiles during switching at various time in terms of fraction of the switching time τ_s at temperature $t = 0.5, \delta_r = 2.0, l = 10.0$ and $e = 0.3$. The number at each curve represents time taken to reach the stage in term of fraction of τ_s . **123**
- Figure 5.8 Hysteresis loops of system of finite size for temperature $t = 0.0, 0.2$, and $0.6. l = 1.8, \delta_r = +3.0, e_0 = 1.0, \omega = 0.01$. **124**
- Figure 6.1 Initial polarization $p(\zeta)$ versus ζ during relaxation for time $\tau_r = 0, 0.1, 0.5, 1.0, 3.0$, and $9.478. t = 0, l = 4, e = 0$. The dotted curve is the stable polarization profile after $\tau_r = 9.478$. **127**
- Figure 6.2 Polarization profiles $p(\zeta)$ versus ζ for film thickness $l = 3.5, 4, 4.5, 5.5, 7.5, 10, 12, 15, 20, 25, 30, 35, 40, 50$ and $60. t = 0.0, e = 0.0$ **128**
- Figure 6.3 Average polarization versus film thickness $l. t = 0, e = 0$. **128**
- Figure 6.4 Average polarization versus time for temperatures $t = 0.0, 0.1, 0.2, 0.3$ and $0.4. e = 0.8, l = 10.0$. The inset shows the corresponding current versus time. **129**
- Figure 6.5 Average polarization versus time for thicknesses $l = 3.5, 4.0, 4.5, 5.5, 7.5, 10, 12, 15, 20, 25, 30, 35, 40, 50$ and $60. t = 0, e = 1.2$. **130**
- Figure 6.6 Switching current vs. time for various film thicknesses l as shown by numbers. $t = 0.0, e = 1.2$. This Figure corresponds to the Fig. 6.5. **131**

Figure 6.7	Switching current versus time for thicknesses $l = 20, 25, 30, 35, 40, 50$ and 60 . $t = 0.0, e = 1.2$. This figure is a part of the Fig. 6.6.	131
Figure 6.8	Polarization profile $p(\zeta)$ during switching for FE film. $l = 3.5$. $t = 0.0, e = 1.2$. The numbers at each curve represents time taken to reach the stage in terms of fraction of $\tau_s = 3.425$.	133
Figure 6.9	Polarization profile $p(\zeta)$ during switching for FE film. $l = 5.5$. $t = 0.0, e = 1.2$. The numbers at each curve represents time taken to reach the stage in terms of fraction of $\tau_s = 4.622$.	133
Figure 6.10	Polarization profile $p(\zeta)$ during switching for FE film. $l = 20.0, t = 0.0, e = 1.2$. The curves are the polarization profile $p(\zeta)$ taken from bottom to top at the time $\tau_r = 0.0, 0.1, 0.2, 0.3, 0.4, 0.5, 0.6, 0.7, 0.8, 0.9$ and 1.0 in terms of fraction of $\tau_s = 7.429$.	134
Figure 6.11	Polarization profile $p(\zeta)$ during switching for FE film. $l = 60$. $t = 0.0, e = 1.2$. The curves are the polarization profile $p(\zeta)$ taken from bottom to top at the time $\tau_r = 0.0, 0.1, 0.2, 0.3, 0.4, 0.5, 0.6, 0.7, 0.8, 0.9$ and 1.0 in terms of fraction of $\tau_s = 8.423$.	134
Figure 6.12	Switching current versus time for film on surface vicinity (dashed curve) at film centre (solid curve) and switching current of average polarization versus time (dotted curve). $l = 5.5, t = 0.0, e = 1.2$.	135
Figure 6.13	Switching current versus time for film on surface vicinity (dashed curve) at film centre (solid curve) and switching current of average polarization versus time (dotted curve). $l = 60.0, t = 0.0, e = 1.2$.	136
Figure 6.14	Switching current versus time for applied field $e = 0.9, 1.2, 2.0$. $l = 60.0, t = 0.0$. The inset shows the zoom in view for switching current versus time under $e = 2.0$.	136
Figure 6.15	Polarization profile $p(\zeta)$ during switching for FE film. $l = 60.0, t = 0.0, e = 2.0$. The numbers at each curve represents time taken to reach the stage in terms of fraction of $\tau_s = 3.515$.	137
Figure 6.16	Switching time τ_s versus applied electric field e for thicknesses $l = 4.0, 5.0, 7.0, \text{ and } 10$. $t = 0.0$. The vertical arrows point to the film coercive field.	138

Figure 6.17	Average polarizations versus e for triangular electric field amplitude $e_0 = 0.26, 0.279, 0.27935, 0.28, 0.29, 1.0, 1.3$ and 2.0 . $l = 4.0, t = 0.0, \omega = 0.06$.	140
Figure 6.18	Average polarization versus e for triangular electric field frequency $\omega = 0.01, 0.06$ and 1.0 . $l = 4.0, t = 0.0, e_0 = 1.0$.	140
Figure 6.19	Average polarization versus e for different temperature $t = 0.7, 0.3$ and 0.0 . $l = 6.0, \omega = 0.08, e_0 = 1.2$.	141
Figure 6.20	Average polarization versus e for film thicknesses $l = 3.5, 5.0$ and 7.0 . $t = 0.0, \omega = 0.08, e_0 = 1.2$	141
Figure 7.1	Schematic diagram of epitaxial film under stress.	144
Figure 7.2	Average polarizations versus temperature for different values of S_m . Solid curves are for six-order potential. Dotted curves are for eight-order potential. Dotted-dashed curve is for stress-free bulk BaTiO ₃ . The curves are calculated for $\delta = 6.56$ nm and $L = 8$ nm.	154
Figure 7.3	Thickness dependence of average polarization for various S_m . Dotted curve for stress-free film. $T = 25^\circ\text{C}, \delta = 6.56$ nm.	156
Figure 7.4	Average polarizations versus misfit strain S_m for different thickness. $T = 25^\circ\text{C}, \delta = 6.56$ nm. The inset shows the zoom in view for a range of $30 \times 10^{-3} \geq S_m \geq 12 \times 10^{-3}$ and $0.325 \leq \bar{P} \leq 0.370$.	156
Figure 7.5	T Transition temperatures versus misfit strain for different thicknesses of strained BaTiO ₃ films. The dashed line is the transition temperature of free-stress bulk BaTiO ₃ (128°C), $\delta = 6.56$ nm.	160
Figure 7.6	Spontaneous polarization $P_s(z)$ versus z for strained BaTiO ₃ film for various strain as indicated by numerals. Solid curve is for stress-free BaTiO ₃ film. Solid straight line is for stress-free bulk and long-dashed straight line is for strained bulk BaTiO ₃ . $L = 12$ nm. $T = 25^\circ\text{C}, \delta = 6.56$ nm.	162
Figure 7.7	Entropy (solid curve) and average polarization (dashed curve) versus temperature for strained BaTiO ₃ bulk. $S_m = -5 \times 10^{-3}$.	163
Figure 7.8	Surface polarization, centre polarization and average polarization versus temperature of strained BaTiO ₃ film. $L = 8$ nm, $S_m = -26 \times 10^{-3}, \delta = 6.56$ nm.	164

Figure A.1 Schematic diagram of components of stresses acting on a cubic faces **188**

Teori Landau Bagi Filem Bebas dan Filem Epitaksi Feroelektrik

Abstrak

Teori Landau-Ginzburg-Devonshire (LGD) dan persamaan dinamik Landau-Khalatnikov telah digunakan untuk mengkaji penyongsangan pengkutuban bagi sistem-sistem feroelektrik (FE) tertib kedua. Sistem-sistem feroelektrik yang dipertimbangkan adalah filem-filem FE yang mempunyai pengkutuban pada permukaan yang terhingga dan juga pada permukaan pengkutuban yang sifar nilainya. Pengkutuban pada permukaan yang sifar tersebut mungkin diakibatkan daripada bahagian yang bukan-feroelektrik di permukaan filem. Sistem FE lain yang dipertimbangkan adalah suatu sistem saiz terhingga berdimensi satu yang terdiri daripada $(2N+1)$ tapak dengan tapak $-N$ dan tapak $+N$ sebagai pinggir. Apabila suatu medan elektrik dikenakan, semua tapak termasuk pinggir juga dikenakan medan yang sama.

Kami menggunakan medan elektrik berbentuk tangga, medan elektrik 'sinusoidal' dan medan elektrik 'bipolar' dalam kajian fenomena pensuisan bagi sistem feroelektrik tersebut. Kesan-kesan kekuatan E_0 dan frekuensi ω bagi medan elektrik yang digunakan, suhu T , ketebalan filem L dan parameter permukaan δ ke atas penyongsangan pengkutuban telah dikaji. Teknik Runge-Kutta (R-K) dan kaedah beza terhingga telah digunakan untuk memperolehi profail pengkutuban awal yang stabil bagi filem berpengkutuban permukaan terhingga dan sistem saiz terhingga. Suatu fungsi percubaan kosinus digunakan untuk memperolehi profail pengkutuban awal bagi suatu filem FE yang mempunyai pengkutuban permukaan sifar.

Kontroversi persandaran ketebalan terhadap medan koersif E_C yang telah dilaporkan dalam kajian eksperimen telah diterangkan secara teoretis yang melalui tanda yang berlainan pada parameter permukaan filem, δ . Bagi kes negatif δ , nilai E_C bertambah terhadap pengurangan ketebalan filem, manakala bagi kes $+\delta$, nilai E_C menurun apabila ketebalan filem berkurangan. Di samping itu, medan koersif didapati juga bersandar kepada ketebalan filem. Dengan menggunakan kaedah penyuaian lengkung ke atas data-data numerik bagi pensuisan filem FE, kami mendapati bahawa masa pensuisan adalah berfungsi eksponen bagi medan yang dikenakan dan fungsi tersebut mengimplikasikan wujudnya medan koersif E_C untuk filem FE. Berdasarkan lengkung ini, ia jelasnya menunjukkan bahawa filem FE akan disuiskan hanya dengan menggunakan medan elektrik E_C yang minimum. Bagi filem FE yang mempunyai pengkutuban permukaan sifar, kami dapati bahawa dua puncak wujud dalam arus pensuisan bagi filem yang agak tebal. Puncak lain yang wujud di dalam arus pensuisan adalah disebabkan momen-momen dwikutub yang berada di permukaan telah disuiskan sebelum momen-momen dwikutub yang berada di dalam filem.

Kesan-kesan keterikan “misfit” terhadap peralihan fasa, pengkutuban purata, suhu peralihan dan ketebalan kritikal bagi filem BaTiO_3 telah dikaji dengan menggunakan tenaga bebas LGD yang mengandungi parameter bertertib sehingga bertertib-lapan oleh sebab ketegasan mampatan yang tinggi hasil daripada antara muka substrak. Fasa peralihan bagi filem epitaksi BT telah didapati bertertib kedua manakala bagi filem BT bebas daripada tegasan, ia adalah berfasa tertib-pertama. Kami mendapati bahawa keterikan “misfit” pada filem BT telah meningkatkan pengkutuban purata dan suhu peralihan dalam filem nipis berketebalan sehingga

1.2 nm. Daripada pengiraan, kami meramalkan ketebalan kritikal bagi filem BT yang terik adalah 0.8 nm.

Landau Theory of Free Standing and Epitaxial Ferroelectric Film

ABSTRACT

Landau-Ginzburg-Devonshire's (LGD) theory and Landau Khalatnikov's dynamic equation are used to study the polarization reversal of second order ferroelectric (FE) systems. These FE systems that we considered are FE films with finite value of surface polarization and also films where the surface polarization can be considered as zero value. This zero surface polarisation could be the result of non-ferroelectric sites present at film surfaces. Another FE system considered is a one dimensional finite size system which is made up of $(2N+1)$ sites with the edges at the $-N^{th}$ and $+N^{th}$ sites. When an external electric field is applied, all the sites including the edges feel the same field.

Various forms of electric fields such as step field, sinusoidal field, triangular field and bipolar field are used to study the switching phenomena in these FE systems. The influence of the amplitude E_0 and frequency ω of the applied electric field, temperature T , film thickness L and surface parameter δ on polarization reversal have been investigated. Runge-Kutta (R-K) method and finite difference technique are the numerical techniques used to obtain the equilibrium initial polarization profile for the film of finite surface polarization and for the system of finite-size. A trial cosine function is used to obtain the initial polarization profile of FE film with zero surface polarization.

The controversial thickness dependence of coercive field E_c in FE film reported in experimental studies, can be explained theoretically by the signs of δ ,

the extrapolation length. For negative δ , E_c increases with decreasing film thickness, while for positive δ , E_c decreases with decreasing film thickness. The coercive field of FE film is found to be thickness dependent. It is interesting to note that the numerical values of switching time and the applied field are best fitted by an exponential function with high regression factor. From this curve, it has clearly shown that the FE film will only be switched by a minimum electric field E_c . Regarding the FE film with zero surface polarization, two peaks in the switching current are found for a relatively thick film. The extra peak in the switching current is due to the dipole moments near the surface are switched earlier than the dipole moments in the interior.

The effects of misfit strain on the phase transition, spontaneous polarization, transition temperatures and critical thickness of epitaxial Barium Titanate BaTiO₃ are examined by using LGD free energy with the order parameter up to the eight-order because of the high compressive stress caused by the substrate interface. Phase transition of epitaxial BaTiO₃ film is found to be of second-order, though the stress-free BaTiO₃ film undergoes first-order phase transition. The misfit strain in BaTiO₃ films increases the average polarization and the transition temperature in films are shown for thicknesses up to the 1.2 nm. From our calculations, we predicted that the critical thickness of strained BaTiO₃ film is 0.8 nm.

Chapter 1

An Overview

1.1 Introduction

A data storage device is a device for recording (storing) information (data). Many different forms of storage, based on various natural phenomena, have been invented. As of 2008, the most commonly used data storage are based on semiconductor, magnetic, and optical technologies. Semiconductor memory uses semiconductor-based integrated circuits to store information. Both volatile and non-volatile forms of semiconductor memory exist. Magnetic storage uses different patterns of magnetization on a magnetically coated surface to store information. Magnetic storage is non-volatile. The typical optical disc, stores information in deformities on the surface of a circular disc and reads this information by illuminating the surface with a laser diode and observing the reflection. Optical disc storage is non-volatile. So far, there is no single storage medium exists for all nature of storage and all forms of storage device currently in used have some drawbacks. Therefore a computer system usually contains several kinds of storage device and each with its purpose.

The spontaneous polarisation in FE can be reversed by applying an external electric field. Hence, FE materials are suitable candidate to be fabricated as a memory device as it is non-volatile. There are many principle advantages of Non-Volatile Ferroelectric Random Access Memories (NV-FeRAMs) such as low operating voltage (1.0 V), small size, radiation hardness, high switching speed (60 ns)

and it has large amount of stored electrical energy from the large remnant polarization P_r in FE materials (Uchino, 2000; Scott, 2000; Lines and Glass, 1977).

There are many problems involved in the fabrication of thin FE film used in NV-FeRAMs. These problems include fatigue, high processing temperature, toxicity, defects, leakage current, destructive read operation, a non well-defined coercive field and unobvious thickness dependence of coercive field. Switching properties of FE thin films such as coercive field E_C and switching time t_s have attracted tremendous scientific and technological interests among the researchers over a long period of time. These properties are directly related to the application of FE films in NV-FeRAMs, where the speed of reversing the remnant polarization at low operating voltages is the main concern in order to produce devices which operate at reduced power and at high switching speed (Scott, 2000; Dawber *et al.*, 2005).

Theoretical studies parallel to experimental investigations of FE materials is a necessity in order to improve the quality of NV-FeRAMs devices produced. Besides the enormous experimental work, theorists have formulated a few models to elucidate on these switching properties of FE thin films, namely the statistical theories such as Kolmogorov-Avrami-Ishibashi model (KAI) (Ishibashi and Takagi, 1971; Orihara and Ishibashi, 1992; Orihara *et al.*, 1994 and Hashimoto *et al.*, 1994), finite grain model (FGM) (Duiker and Beale, 1990), Nucleation-limited-switching model (NLS) (X. Du and I.-W, 1998; Lohse *et al.*, 2001; Colla *et al.*, 1998a; Ganpule *et al.*, 2000; Tagantsev *et al.*, 2002) and Lorentzian distribution model (Jo *et al.*, 2007). Other models found in the literature are based on Landau-typed theory such as the discrete lattice model (Ishibashi, 1990; Ishibashi, 1992)). However, there are many other approaches discussed on the polarisation reversal such as the classical Landauer model (Landauer, 1957; Gerra *et al.*, 2005) and phase-field model

(Choudhury *et al.*, 2007). Strictly speaking, neither the statistical models nor the Landau discrete model of Ishibashi and other approaches that we have mentioned have taken into consideration of the effects of surface on polarisation reversal in FE films.

The Landau theory has been used as a theoretical background for studies of many systems in condensed matter which undergo phase transition; such as superconductors, ferromagnets, liquid crystals and ferroelectrics. The Landau theory, a phenomenological theory which takes into consideration of the thermodynamics, was perfected for bulk FE by Ginzburg (1949 cited in Lines and Glass, 1977) and Devonshire (1949 cited in Gonzalo, 2005) by assuming that in the FE system, the same energy function is capable of describing both polar and non-polar phases. Landau-Ginzburg-Devonshire theory (LGD) has been used successfully in studying thin films of ferroelectrics since 1979 (Kretschmer and Binder, 1979).

The main aim of this thesis is to examine the properties of switching phenomena for different FE systems by using LGD free energy equation and Landau Khalatnikov's dynamic equation and taking into account of the surface effect on FE films. A discrete form of LGD equation is used to study FE systems of finite size made up of $(2N+1)$ sites with the $-N^{th}$ and $+N^{th}$ sites as edges (Ishibashi *et al.*, 2007). While, a continuum form of LGD equation is used to examine FE films with zero value of surface polarisation which could be the result of non-ferroelectric sites present at film surfaces. And the continuum LGD equation of Tilley-Zeks model (Tilley and Zeks, 1984) is used to investigate FE films with finite values of surface polarisation. Tilley-Zeks model has been used successfully in describing phase transition and dielectric properties of FE thin films (Ong *et al.*, 2001; Zhong *et al.*,

1994a). In this model, surface effects are represented by the extrapolation length $\pm\delta$, where $+\delta$ represents the suppressed polarisation at the surfaces and $-\delta$ represents the enhancement of surface polarization.

In another part of this thesis, the phase transition properties of thin epitaxial strained ferroelectrics film of Barium Titanate BaTiO₃ are examined by using the LGD theory. Epitaxial BaTiO₃ film can be markedly different from the intrinsic properties of the corresponding unstrained material. Experimentally, it is found that strain offers the opportunity to enhance the polarisation and also increases the transition temperature. (Forsbergh, 1954; Terauchi *et al.*, 1992; Yoneda *et al.*, 1993, 1998; Yano *et al.*, 1994; Yanase *et al.*, 1999; Choi *et al.*, 2004; Kim Y. S. *et al.*, 2005). Theoretically, many studies have been done to investigate the phase transition properties of epitaxial ferroelectrics film of BaTiO₃ (Pertsev *et al.*, 1998; Zembilgotov *et al.*, 2002; Pertsev and Kohlstedt, 2007). One of these studies (Zembilgotov *et al.*, 2002) employed LGD potential of six-order polynomial to investigate the phase transition properties of epitaxial BaTiO₃ film while others ignore the surface effect (Pertsev and Kohlstedt, 2007). In this thesis we are motivated to investigate the polarisation properties of epitaxial BaTiO₃ thin film by using LGD free energy which includes eight-order term in the polynomial and the surface effect. Surface effect is significant in ultra thin film.

1.2 Thesis Overview

The physics of ferroelectrics is dealt with in chapter 2, whereas chapter 3 is the literature review on the theoretical and experimental studies of switching phenomena of FE films and epitaxial films. Chapter 4 investigates the polarisation reversal of second-order FE thin film by using Tilley-Zeks model. Effects of thickness and

surface are taken into account in modeling the Landau free energy. A new formula which relates the switching time to electric field is obtained through curve-fitting. The results predicted the existence of a coercive field in the system of FE films. We devote chapter 5 to study the switching phenomena of FE discrete system of $(2N+1)$ sites with the $-N^{th}$ and $+N^{th}$ sites as edges. All the sites of the system are assumed to feel the same applied electric field. Chapter 6 discusses the polarisation reversal of FE thin films with zero-surface polarisation. The phase transition properties of epitaxial thin films of $BaTiO_3$ are discussed in chapter 7. An eight order term is added to the free energy polynomial. A critical thickness is found in this study for $BaTiO_3$. Conclusions and possible extensions to our work are presented in chapter 8.

Chapter 2

General Physics of Ferroelectric

2.1 Definition of Ferroelectricity

According to the geometry, crystals are classified into seven systems: triclinic, monoclinic, orthorhombic, tetragonal, trigonal, hexagonal, and cubic. Depending on crystals symmetry with respect to a point, there are 32 crystal point groups. Eleven of them possess a centre of symmetry and that means an applied uniform stress on these crystals produce symmetrical movements around the centre of symmetry. An applied electrical field on these crystals produces a strain, which remains unchanged when the field is reversed.

The 21 remaining non-centrosymmetric crystal point groups, except 1 possess polarity under stress or strain under electric field. The effect is linear and it is called piezoelectricity. Ten of these piezoelectric materials have unique polar axis with temperature-dependent spontaneous polarisation. These ten materials are pyroelectric materials (Lines and Glass, 1977).

Ferroelectric materials are dielectric materials which belong to the pyroelectric group. Ferroelectric materials have spontaneous polarisation P_s which is in at least two directions. P_s can be reversed by applying an external electric field. Due to this reversibility, the ferroelectric form a distinct subclass of the pyroelectric. At a certain critical temperature called transition temperature T_C , a ferroelectric material undergoes phase transition from ferroelectric phase with non-zero P_s to paraelectric

phase where magnitude of P_s equals zero. Typical ferroelectric materials possess P_s which decreases with increasing temperature T and to disappear continuously (second-order transition) or more often discontinuously (first-order transition) at T_C . However, transition from paraelectric phase to ferroelectric phase as a function of increasing temperature can occasionally occur (Känzig, 1957; Jona and Shirane, 1962; Lines and Glass, 1977).

2.2 Brief History of Ferroelectricity

Valasek (1920, 1921) discovered that the spontaneous polarisation of sodium potassium tartrate tetrahydrate $\text{NaKC}_4\text{H}_4\text{O}_6 \cdot 4\text{H}_2\text{O}$ better known as Rochelle salt could be reversed by application of an external electric field. He discovered ferroelectricity through experiments which showed that the dielectric properties of this crystal are similar in nature to the ferromagnetic properties of iron such as appearance of hysteresis loop in the field-polarisation curve, a Curie temperature T_C and possess an extremely large dielectric response around the critical temperature. In 1935 to 1938 the first series of ferroelectric crystals were produced in Zurich (Busch, 1938). These series of crystals were phosphates and arsenates, of which the principle example is potassium dihydrogen phosphate KH_2PO_4 . In 1945 BaTiO_3 ceramic was found to have ferroelectricity (Lines and Glass, 1977). This discovery is important because this material is the first ferroelectric material discovered which has no hydrogen bond; and it has more than one ferroelectric phase transitions. The prototype structure BaTiO_3 is cubic centrosymmetric perovskite with only five atoms per unit cell. This structure is simple and is chemically and mechanically very stable. It is ferroelectric at room temperature, and can be easily prepared and used in

ceramic form. BaTiO_3 soon became the most extensively investigated ferroelectric material (Cross and Newnham, 1987).

The discovery of ferroelectric materials subsequently leads to some basic theories being proposed. Slater (1941) presented the first basic microscopic model for ferroelectrics after KH_2PO_4 was discovered. It was thought that the existence of hydrogen bond in ferroelectric materials such as KH_2PO_4 was a necessary, if not sufficient condition for the polar instability to occur. Slater's model assumed the ordering of the hydrogen atoms corresponds to the polar phase of ferroelectricity. The hydrogen hypothesis of ferroelectricity has to be abandoned after the discovery of perovskites such as BaTiO_3 and Lead Titanate PbTiO_3 which have no hydrogen bond. Mueller (1940a, 1940b) applied thermodynamics in the study of ferroelectric properties in Rochelle salt. The idea was to write the free energy of ferroelectric material as power series of polarisation and strain. The success of the theory therefore lies in the fact that at a certain temperature, it is capable of explaining dielectric, piezoelectric, and elastic behaviours from a limited number of terms in the free-energy polynomial. This thermodynamic macroscopic theory was perfected by Ginzburg (1949 cited in Lines and Glass, 1977) and by Devonshire (1949 cited in Gonzalo, 2005) by assuming that the same energy function is capable of describing both polar and non-polar phases.

In order to explain the behaviour of displacive-type FE, Slater (1950) assumed that the ferroelectric behaviour of perovskite materials such as BaTiO_3 are caused by the long-range dipolar forces which tend to destabilize the high-symmetry configuration favoured by the local forces. This model has first assumed that the titanium ions Ti^{+4} move in a rigid frame work from the rest of the lattice. Later, Anderson (1960) and Cochran (1960) (as cited in Lines and Glass, 1977) realized

that this theory could be casted within the frame work of lattice dynamic (soft-mode) involving the ionic motion of all the constituent atoms to describe the displacive lattice instability. Over the period of 1960s to 1970s, the full weight of information from experimental work on inelastic neutron, Raman, Brillouin, and Rayleigh scatterings were used to verify and extend the soft-mode description.

2.3 Ferroelectric Domains

The most important property of a ferroelectric is the reversibility of its spontaneous polarisation. It is necessary to understand the ferroelectric domain first in order to understand the polarisation reversal. Usually the ferroelectric crystal is not polarized uniformly in one direction, but the polarisation is composed of many regions called domains. A domain is an ordered region, and the extent of the ordering in different domains can be the same. Each domain contains a large number of dipoles all aligned in the same direction (Jona and Shirane, 1962). The magnitude of polarisation may be the same in different domains, even though the directions are not. It is quite possible, however, for the magnitudes of polarisation to differ because of stress and field set up by neighbouring domains (Burfoot, 1967). The direction of polarisation inside a domain can be normal to the (001) plane and this domain is called 'c' domain. While if the polarisation lies within the (001) plane, the corresponding domain is called 'a' domain. Fig. 2.1a shows a schematic diagram of 'a' domain between two 'c' domains, while Fig. 2.1b shows a schematic diagram of 'a' domains.

The most common structure of domains in ferroelectric materials is antiparallel domains (Fig. 2.2). The antiparallel domains are formed due to the effect of depolarization field E_d . The depolarization field is created by bound charges

induced on the external surfaces of a single domain (Jona and Shirane, 1962). In other words, depolarization field appears at the surface where P_S is suppressed or in the neighbourhood of defects (not perfect crystal) where there is spatial variation of P_S (Lines and Glass, 1977). The energy of depolarisation field W_E is proportional to the square of P_S . Since $W_E = \vec{P} \cdot \vec{E}_d$, so in an insulated crystal, W_E may reach a very high value in a short time. In order to minimize this energy, the single domain splits into many antiparallel domains, a state which is energetically more stable because it reduces the depolarization field. Fig. 2.2 shows that the presence of antiparallel domains with respect to the depolarization field reduces the value of E_d . This domains splitting will not proceed indefinitely because a certain amount of energy is stored in the boundary layers called the domain walls. When the overall domain wall energy has increased to a point which balances the decrease in energy of the depolarization field, then an equilibrium configuration is reached. This is the stable domain configuration at the temperature considered (Jona and Shirane, 1962). However a real ferroelectric is never an ideal insulator, so the bound charges induced by P_S at the surfaces are partially compensated by the bulk and surface conductivity, and this may partially reduce E_d or E_d may vanish completely. In highly conducting ferroelectrics, single-domain formation seems to be preferred (Didomenico and Wemple, 1967).

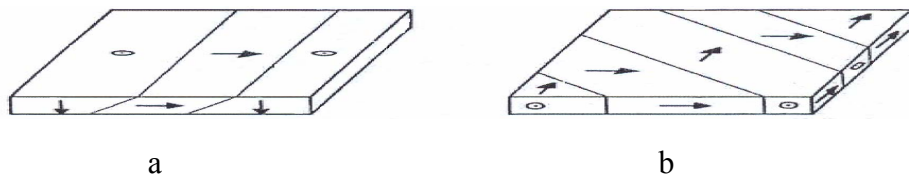


Figure 2.1 Schematic diagram of domain arrangements in (001) plate of tetragonal BaTiO₃. Arrows represent the direction of the polar axis. (a) is for 'a' domain between 'c' domains, (b) is 'a' domains only.

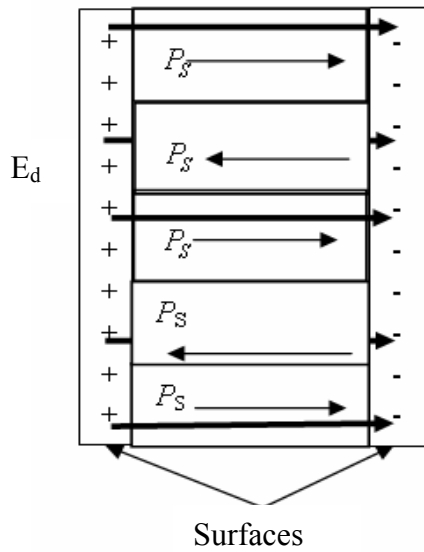


Figure 2.2 Schematic diagram of antiparallel domains formed as a result of depolarization field E_d (thick arrows) due to bound charges on surfaces. Thin arrows are for P_s . Surfaces here are the domain boundary of ferroelectric without external electrodes.

The thickness of a domain wall is a result of the compromise between two opposing energies: the exchanged energy and the anisotropic energy of the dipoles. The exchanged energy between two neighbouring dipoles is proportional to the square of the angle between the order parameter P_s and it tends to broaden the wall. While the anisotropic energy is the energy cost to deviate the polarisation vector from the preferred axes (ferroelectric axes) (Känzig, 1957). Since the word “domain” is borrowed from the study of ferromagnetism, it is worth to have a comparison between ferromagnetic and ferroelectric domains. Table 2.1 and Fig. 2.3 show a comparison between ferromagnetic and ferroelectric domains (Jona and Shirane, 1962).

Table 2.1 Domain wall configurations: a comparison between ferromagnetic and ferroelectric domain

	Ferromagnetic domain	Ferroelectric domain
1.	Domain wall is a transition region in which the magnetization vector turns over gradually from a given direction to the opposite one. See Fig. 2.3a	Spontaneous polarisation preserves its axis as the domain traversed. The polarisation vector will not rotate but rather will decrease in magnitude passing through zero, and increase on the other side with opposite sign. See Fig. 2.3b
2.	Exchange energy \gg anisotropy energy (spins in many directions), so the domain wall is thick	No real exchange energy, the interaction energies of parallel and antiparallel dipole arrays do not differ much from each other thus a narrow domain wall is favoured. The anisotropy is so high: P_s can hardly deviate from that of the ferroelectric axis except at temperature near T_C , at which the ferroelectric axis changes its direction.
3.	No strain effect	Piezoelectric effect (strain caused by the polarisation) prefers a thin domain wall
4.	Thick domain wall (300 lattice constant)	Narrow domain wall (one lattice constant)

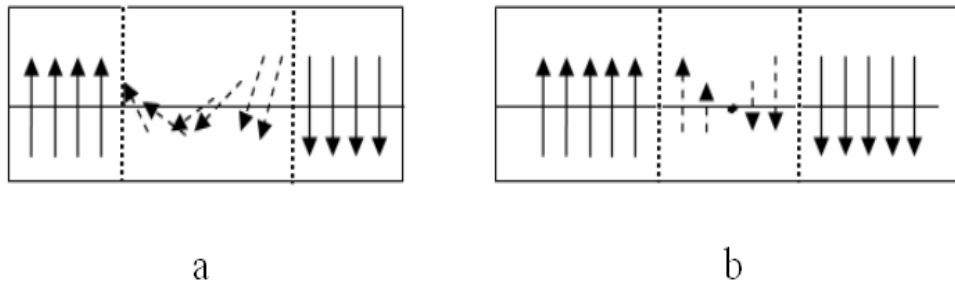


Figure 2.3 Schematic diagram showing the difference between ferromagnetic and ferroelectric 180° domains. (a) for ferromagnetic, (b) for ferroelectric. The layer between the dotted lines is the thickness of the domain wall (Jona and Shirane, 1962).

Figure 2.4 shows the schematic diagram of domain walls for tetragonal structure of BaTiO_3 . BaTiO_3 has a cubic structure in paraelectric phase, upon cooling the crystal of BaTiO_3 below the Curie temperature T_C ($T_C = 120^\circ$) the structure of the crystal becomes tetragonal as a result of the cubic edges along c -axis are elongated, while other cubic edges are compressed. There are six possible directions of domains which coincide with three pairs of antiparallel directions along the cube edge. The polar axis can be parallel to any one of these six equivalent directions. This gives rise to two different types of walls, namely those separating antiparallel dipoles (180° walls) and those separating dipoles at right angles to each other (90° walls). The schematic diagrams are shown in Fig. 2.4. The thicknesses of 180° walls in BaTiO_3 are believed to be in the order of one lattice spacing. So, a dipole can reverse its sign within one unit-cell distance, and thus the periodicity of the lattice is practically undisturbed (Burfoot, 1967). Usually the 90° domain wall is thicker than 180° domain wall as seen in Fig. 2.4. The 180° wall is usually so thin that it has a much smaller volume than the bulk domains (Burfoot, 1967).

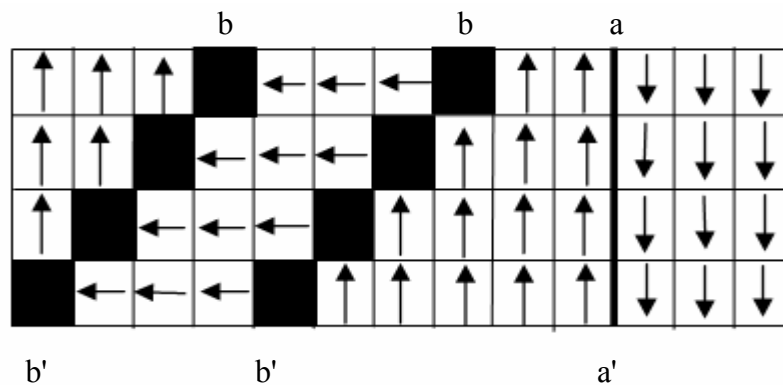


Figure 2.4 Schematic diagram of domain walls for tetragonal BaTiO_3 . (a-a') is 180° wall, (b-b') are 90° wall (Jona and Shirane, 1962).

2.4 Switching Phenomenon

The characteristics of switching phenomenon in ferroelectric materials can be understood with reference to a fictitious one-dimensional crystal made up of two atoms of opposite charges shown in Fig. 2.5. In this crystal, it is clear that we can orient the dipoles to point all to the right, or all to the left. The two structures are completely equivalent; except that they have opposite signs to the dipole moments. They must therefore have exactly the same energy. We could transform one structure into the other by dragging one type of atom towards the other. As we do this, the bulk polarisation will be reduced in magnitude, and changes sign at the point where the atoms are equally spaced and finally switch to the opposite direction. Given that we know the crystal is stable in either of the two polarized states, there must be an energy barrier between the two states, and we can sketch a curve (Fig. 2.6) for the energy as a function of the polarisation. The curve shows the symmetrical double potential well

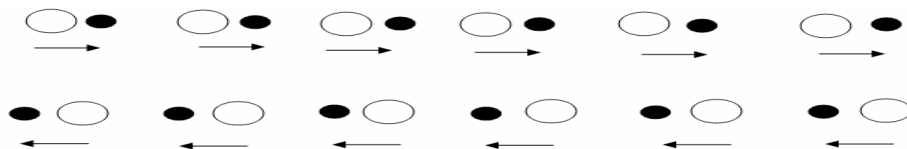


Figure 2.5 One dimensional fictitious crystal (Jona and Shirane, 1962)

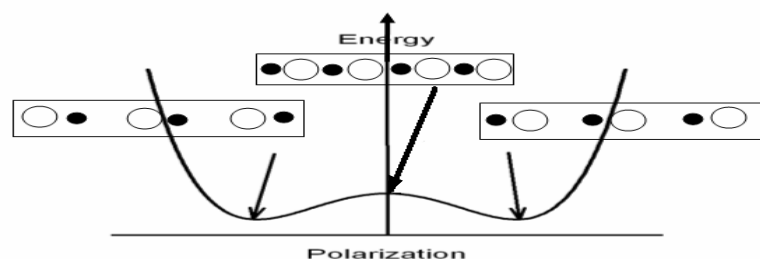


Figure 2.6 Schematic diagram of double potential wells

If an electric field E is applied, the two stable states no longer having the same energy because of the energy due to the coupling of electric field and polarisation $-P_s E$. The potential wells are tilted by the electrical field. From Fig. 2.6 it shows that a small field will not immediately switch the polarisation from one direction to the other because there is a barrier to be overcome. When a sinusoidal or a triangular electric field is applied, all the dipoles have to be reversed for switching to take place. However, in a real material not all the microscopic dipoles will uniformly switch together (Jona and Shirane, 1962; Strukov and Levanyuk, 1998).

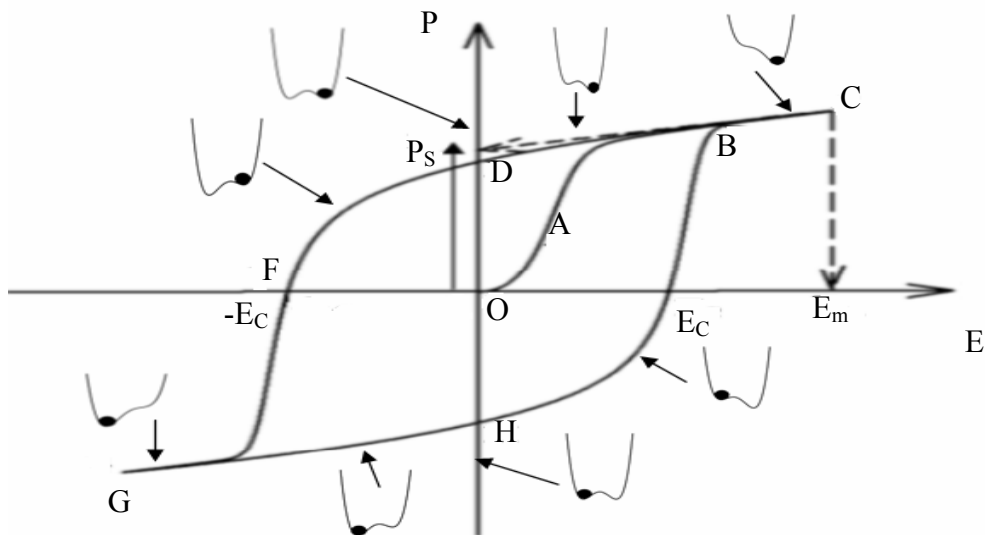


Figure 2.7 Schematic representation of P - E hysteresis loop of a second order ferroelectric material. The double potential wells represent the state of minimum polarisation during switching.

The following steps explain the formation of hysteresis loop (Fig. 2.7) of ferroelectricity:

- I. In a fresh crystal (a crystal which has an equal number of negative and positive domains) the net polarisation P is zero (point O).

- II. When a small electric field E is applied in a positive direction, the net polarisation increases almost linearly with E like in a normal dielectric material (OA) (Connolly and Turner, 1970).
- III. By increasing E , in a positive direction, the negative polarisations start to switch over in the positive direction rapidly (AB). This switching continues until all negative polarisations are aligned in the positive direction (BC). The crystal becomes single-domain. The portion (BC) shows the induced polarisation which is linear with the applied electric field.
- IV. By decreasing the positive value of E , the value of polarisation will not return to zero value but follows the path (CD). At $E = 0.0$ the crystal has the remnant polarisation P_r (OD) with a positive direction. While the extrapolation of the linear portion (BC) to the P -axis is called the spontaneous polarisation P_s .
- V. Reversing the direction of applied field will reduce the magnitude of the polarisation until the polarisation value equals zero (point F). The value of the applied field at point F is called the coercive field E_C . It is defined as the critical field which makes the antiparallel orientation of polarisation unstable. It is obvious that the change of E sign will not immediately change the direction of P .
- VI. Increasing E in the negative direction below $-E_C$, the switching of polarisation starts to expand. In the portion (FG), P is in the negative direction, so again we have a single domain crystal.
- VII. The negative polarisation at the point G can be switched to positive polarisation at C through the path GHC .

On the other hand, by applying a step electric field of large enough magnitude (Fatuzzo and Merz, 1967) on Sawyer-Tower circuit (Sawyer and Tower, 1930) which consist of a ferroelectric sample in series with a resistor, the spontaneous polarisation reverses and displacement current (switching current) flows in the crystal. The polarisation reversal is a consequence of the motion of domain walls under the applied electrical field. From the investigation of the polarisation reversal on BaTiO₃, Merz (1954) proposed a mechanism of polarisation reversal where domains are first formed, mainly at the surface. Then grow forward through the sample, and after that the domains begin to expand sideways. These domains coalesce until the entire crystal forms a single domain. More details and comprehensive discussion of polarisation reversal can be found in many standard books (Lines and Glass, 1977; Fatuzzo and Merz, 1967; Jona and Shirane, 1962; Strukov and Levanyuk, 1998; Burfoot, 1967)

2.5 Classification of Ferroelectric Materials

The number of known ferroelectric crystals has increased to an extent that ferroelectricity appears to be a common phenomenon; and a satisfactory classification of all the materials has become very difficult. However, ferroelectrics can be classified as follows:

- I. Ferroelectrics are classified into two groups according to the number of allowed directions of spontaneous polarisation P_s : A group has a single axis of P_s , i.e. the ferroelectrics can be polarized only along one axis such as KH₂PO₄. Another group of ferroelectrics which can be polarized along several axes that are crystallographic equivalent in non-polar phase, such as BaTiO₃. This classification is useful for domain study.

- II. It can be classified according to the existence of a centre of symmetry in non polar-phase. Materials without centrosymmetric in non polar-phase such as KH_2PO_4 and its isomorphous compounds; and with centrosymmetric in non polar-phase such as BaTiO_3 and triglycine sulfate $(\text{CH}_2\text{NH}_2\text{COOH})_3 \cdot \text{H}_2\text{SO}_4$. This classification is useful for the thermodynamic treatment of ferroelectric phase transition.
- III. The other classification depends on the nature of phase change occurring at the Curie point such as order-disorder type such as KH_2PO_4 , triglycine sulfate and sodium nitrite (NaNO_2) and displacive types like BaTiO_3 and most of the double oxide ferroelectrics.

Details on the classifications of ferroelectrics can be found in many books (Jona and Shirane, 1962; Lines and Glass, 1977). We will focus on two major groups of ferroelectrics, the displacive perovskite-type and the order-disorder group.

2.5.1 Displacive Ferroelectrics

Three main types of displacive ferroelectrics are discovered; namely, lithium niobate type (e.g LiNbO_3 , the tungsten bronze type (e.g PbTa_2O_6) and the perovskite type (e.g BaTiO_3 , KNbO_3 , PbTiO_3 , SrTiO_3 and KTaO_3). The group that has been studied intensively is the perovskite group. The structure of perovskite is common to a large family of compounds with the general formula ABO_3 where A is a monovalent, divalent or trivalent metal and B a pentavalent, tetravalent or trivalent elements whose representative in nature is the mineral CaTiO_3 called perovskite. The symmetry of non-polar phase of perovskite ferroelectrics is cubic close-packed with the arrangement of A and O ions together with B ions filling the interstitial

positions. Thus, it is centrosymmetric and non piezoelectric. Fig 2.8 shows the unit cell of the cubic perovskite-type lattice (Jona and Shirane, 1962).

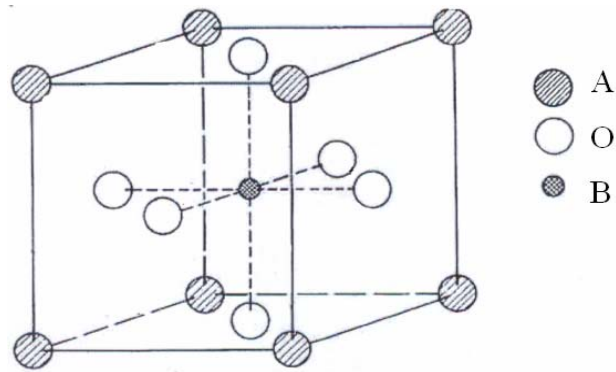


Figure 2.8 Cubic perovskites-type structure.

The perovskite structure can also be regarded as a three-dimensional framework of a set of BO_6 octahedra arranged in a simple cubic pattern, with A atoms occupying the space in between (Lines and Glass, 1977). The arrangement of the BO_6 octahedra provides an infinite linear chain $B-O-B-O-B$ along the $[001]$ directions (Jona and Shirane, 1962). This arrangement has been shown to favour for the action of long-range forces such as dipole interaction and thus for the occurrence of the phenomenon of ferroelectricity. In other words, the spontaneous polarisation in the perovskite ferroelectrics and other types of displacive ferroelectric is due to the displacement of the B ions from its central position in the octahedron

BaTiO_3 is the typical example of perovskite. It has the non-polar cubic perovskite structure ($m3m$) above. Below 120°C it undergoes three ferroelectric phases: first to tetragonal ($4mm$), the atoms shift along the fourfold-axis $[001]$, then

to orthorhombic ($mm2$) at 0°C with polar axis parallel to $[011]$. In some cases it is convenient to retain axes almost parallel to the original cubic edge, so the unit cell has monoclinic geometry, and finally to rhombohedral (trigonal) ($3m$) phase below -70°C with polar axis along $[111]$. All these three transitions are of the first order transition (Lines and Glass, 1977; Strukov and Levanyuk, 1998). Fig. 2.9 shows the three phase transitions of BaTiO_3 and its temperature dependence spontaneous polarisation.

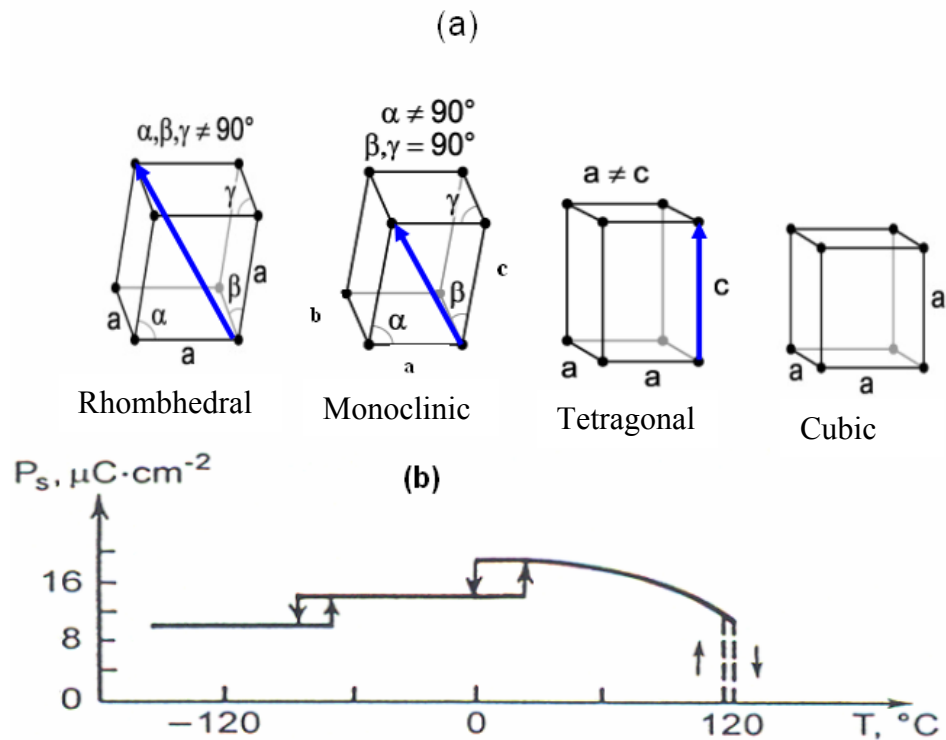


Figure 2.9 Three phase transitions of BaTiO_3 . (a) change of polarisation direction from non polar (cubic) to $[001]$ (tetragonal) to $[011]$ (monoclinic) to $[111]$ (rhombohedral) directions, while (b) the temperature dependence of spontaneous polarisation for the three transitions. The source of (b) from (Strukov and Levanyuk, 1998).

2.5.2 Order–Disorder Ferroelectrics

This type of ferroelectric materials undergoes polar phase transition associated with the ordering of protons in hydrogen bonds. Crystals of sodium nitrite, KH_2PO_4 and triglycine sulfate are typical representatives of ferroelectrics with a phase transition of the order-disorder type (Strukov and Levanyuk, 1998). A lot of details describing the phase transition about order–disorder ferroelectrics can be found in many books (Jona and Shirane, 1962; Fatuzzo and Merz, 1967; Mitsui *et al.*, 1976; Lines and Glass, 1977; Strukov and Levanyuk, 1998).

2.5.2.(a) Potassium Dihydrogen Phosphate KH_2PO_4

The crystal structure of KH_2PO_4 is tetragonal at room temperature. This phase is non-centrosymmetric, therefore KH_2PO_4 is piezoelectric. KH_2PO_4 is in a ferroelectric phase at 123 K with orthorhombic symmetry. KH_2PO_4 undergoes first-order phase transition close to a second-order one (Jona and Shirane, 1962; Lines and Glass, 1977; Strukov and Levanyuk, 1998). The polar axis lies along the direction of the c -axis of the tetragonal phase. The structure of KH_2PO_4 in tetragonal phase is depicted in Fig. 2.10. Each phosphorous atom is surrounded by four oxygen atoms at the corners of a tetrahedron which is almost regular. The structure of KH_2PO_4 is built in such a way that Potassium K and phosphorous P atoms are alternately located at a distance with $c/2$ in the direction of c -axis. Every PO_4 group is linked to four other PO_4 groups with spacing of $c/4$ along c -axis, by hydrogen bonds (Fig 2.11) (Jona and Shirane, 1962).

The overall picture of the phase transition occurring in KH_2PO_4 , obtained both from X -ray and neutron studies, reveals the role played by the hydrogen atoms in the co-operative phenomenon which leads to ferroelectricity. As a rule, hydrogen bonds

do not introduce a direct contribution to spontaneous polarisation as they are oriented at an angle close to 90° in the direction of spontaneous polarisation induced by displacement of other ions (K, P) along c -axis in the opposite direction with reference to O atom (Jona and Shirane, 1962). But the ordering of protons on hydrogen bonds serves as a “triggering mechanism” of a phase transition (Strukov and Levanyuk, 1998).

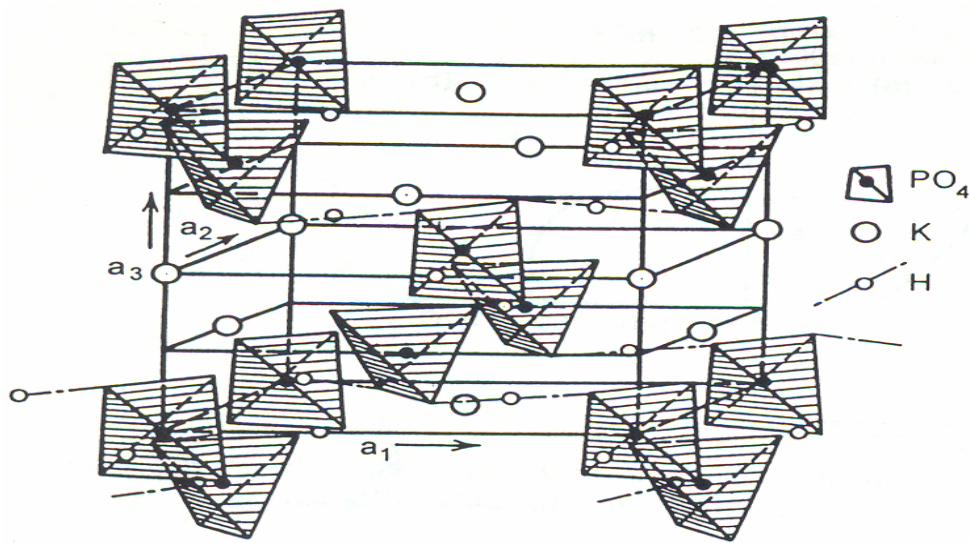


Figure 2.10 Structure of KH_2PO_4 in paraelectric phase.

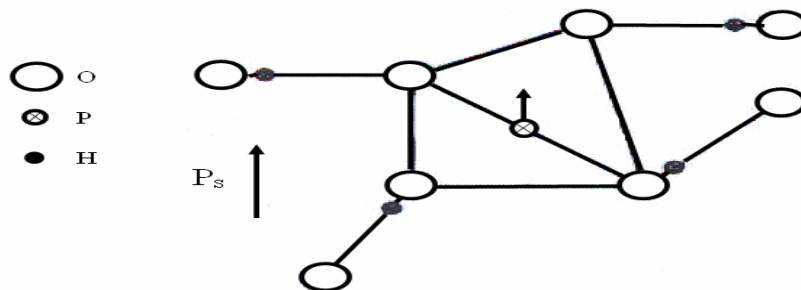


Figure 2.11 PO_4 tetrahedron of KH_2PO_4 structure with hydrogen bonds to the nearest neighbours.

2.5.2.(b) Triglycine Sulfate $(\text{CH}_2\text{NH}_2\text{COOH})_3 \cdot \text{H}_2\text{SO}_4$

Triglycine sulfate is an important order-disorder ferroelectric that exhibits a second-order phase transition. Above the Curie temperature $T_C = 49^\circ\text{C}$ the crystal has monoclinic structure and it belongs to centrosymmetric symmetry of $2/m$. Below T_C , the mirror plane disappears and the crystal belongs to the polar point group 2 of the monoclinic system (Lines and Glass, 1977). The triglycine sulfate structure is complex. It is a net of glycine molecules $\text{CH}_2\text{NH}_2\text{COOH}$ and SO_4 tetrahedra linked together by hydrogen bonds. The glycine groups are asymmetric and possess significant dipole moments in ferroelectric phase. The ordering of protons on hydrogen bonds that link the glycine groups contributes to ferroelectricity in triglycine sulfate (Strukov and Levanyuk, 1998).

2.6 Theories of Ferroelectric Phase Transition

Ferroelectric phase transition is a structural phase transition. It can be treated both microscopically through the lattice dynamical (soft mode) theory and macroscopically through thermodynamic theory in parallel with phenomenological Landau-theory.

2.6.1 Lattice Dynamic Theory of Ferroelectrics

In the fifties and sixties of the last century, research in the field of ferroelectricity underwent a profound change. The central cause of this change is the introduction of the idea that ferroelectric phase transitions are due to instability of the crystal lattice against a low-frequency lattice motion (soft mode) (Blinic and Zeks, 1974).

Slater (1950) assumed that the ferroelectric behaviour of displacive ferroelectric BaTiO_3 was caused by the long-range dipolar forces which tend to destabilize the high-symmetric configuration preferred by the local forces (Lorentz local effective field). One of the main problems of the Slater's model of BaTiO_3 is the assumption that one could focus on the motion of the titanium ion Ti in a rigid framework of the lattice (Lines and Glass, 1977). This problem was successfully overcome by Anderson and Cochran (Cochran, 1960). Anderson and Cochran realized that the Slater's theory should be modified within the frame of lattice dynamic, and one should focus on the lowering of frequency of the transverse optical lattice mode TO ('soft' mode) involving the ionic motions of all constituent atoms to describe the displacive lattice instability of ferroelectrics.

In Lattice dynamic theory, the frequency of the relevant soft phonon decreases on approaching the critical temperature T_C and the restoring force for the mode displacement tends to move to zero until the phonon has condensed out at the stability limit. The static atomic displacements in the material in the transition from paraelectric to the ferroelectric phase represents the frozen-in mode of displacement of the unstable phonon that induces the spontaneous polarisation (Binc and Zeks, 1974).

In the order-disorder ferroelectrics, the 'soft' mode is no longer a crystal vibrational mode but a pseudo-spin wave that describes the motion of protons in the double-potential like hydrogen bond. The pseudo-spin Hamiltonian considers the hydrogen bond as a double-well potential with two possible states of protons in the double-well potential, similar to spin up and spin down states of a $\frac{1}{2}$ spin particle. The interaction between neighbouring double wells is treated as an exchange-type coupling between the pseudo spin. Ising Model in a Transverse Field (IMTF)